

Magnetization and magnetoresistance in insulating phases of $\text{SrFeO}_{3-\delta}$

S. Srinath,¹ M. Mahesh Kumar,² M. L. Post,² and H. Srikanth^{1,*}

¹Materials Physics Laboratory, Department of Physics, University of South Florida, Tampa, Florida 33620, USA

²Institute for Chemical Process and Environmental Technology, National Research Council of Canada, Ottawa, ON, Canada, K1A 0R6

(Received 14 January 2005; revised manuscript received 10 May 2005; published 17 August 2005)

Two insulating phases of $\text{SrFeO}_{3-\delta}$ have been found by the introduction of oxygen deficiencies in metallic SrFeO_3 , one with $0.15 \leq \delta \leq 0.19$ (Sample A) and the other above $\delta=0.19$ (Sample B). Sample A shows large negative magnetoresistance around the charge ordering temperature (CO) associated with a magnetic anomaly. A three-dimensional variable range hopping associated with a localized moment antiferromagnetic behavior was seen in Sample B without any measurable CO down to 70 K. Ac and dc susceptibilities (χ_{ac} and χ_{dc}) show multiple magnetic anomalies associated with a frustrated magnetic order with competing ferro- and antiferromagnetic interactions. The frustration decreases with increasing content of Fe^{3+} , the direct consequence of which is the dilution of helical magnetic spin ordering. The competing effects of ferro- and antiferromagnetic phases extend up to high temperatures $T \sim 230$ K revealing a characteristic temperature scale not known earlier. These observations are discussed in the context of magnetic interactions associated with $\text{Fe}^{4+}/\text{Fe}^{3+}$.

DOI: [10.1103/PhysRevB.72.054425](https://doi.org/10.1103/PhysRevB.72.054425)

PACS number(s): 75.30.-m, 75.30.Kz, 75.47.-m, 75.30.Cr

I. INTRODUCTION

Recent interest in materials which show colossal magnetoresistance (CMR) stems from their ability to produce large changes in resistance with the application of magnetic fields. These materials have also generally displayed a rich phase diagram with intricate coupling between electronic, magnetic, and structural properties.¹⁻⁵ Among the very few materials that show coexistence of charge ordering and ferromagnetism with a metallic phase, $\text{PrCa}_{1-x}\text{Mn}_x\text{O}_{3-\delta}$ is notable.⁶ Compounds of the Ruddlesden-Popper (RP) type, which are close to the manganites, fall into a category of materials with similar magnetic properties.⁷ In particular, RP phases with Fe^{4+} in a high spin state offer an interesting counterpart in ferrates.⁸

In the RP class of systems SrFeO_3 belongs to a category where the structural morphologies critically depend on the oxygen stoichiometry.^{9,10} The charge ratio, Fe^{4+} to Fe^{3+} imparts a profound influence on the magnetic structure and originating properties in $\text{SrFeO}_{3-\delta}$. Stoichiometric SrFeO_3 is an antiferromagnet ($T_N \sim 140$ K) with a cubic perovskite structure at room temperature. An important feature of this ferrate is that it has a helical magnetic spin structure with a propagation vector parallel to the crystallographic (111) plane and shows no Jahn-Teller (JT) distortion even at very low temperatures.^{7,11} SrFeO_3 however is metallic unlike its counterparts in manganites, with strong covalency having the e_g^* orbitals extended into the itinerant conduction band with low electron densities around the nucleus.¹² Recently, it was shown by Lebon *et al.* that in certain oxygen deficient compositions of $\text{SrFeO}_{3-\delta}$, a charge ordered (CO) state with a giant negative magnetoresistance could be observed and was attributed to the $\text{Fe}^{4+}-\text{Fe}^{3+}$ charge ordering.¹³ The metal-insulator transition occurs around $\delta=0.15$ with a magnetic transition around 70 K. With the additional loss of oxygen ($\delta=0.19$), an insulating behavior was seen with a large positive magnetoresistance at low temperatures and negative magnetoresistance near the magnetic transition (60 K). Two

facts that are unclear in the above study are (a) the precise oxygen stoichiometry where the metallic SrFeO_3 transforms to a non-stoichiometric charge ordered insulator and (b) the nature of the intermediate composition bounded by stoichiometries that display metal-insulator transition ($\delta=0.15$) and partly insulating behavior ($\delta=0.19$). Our present investigation addresses these issues and attempts to isolate the intermediate phases (between $\delta=0.15$ and 0.19) and one above $\delta=0.19$ in $\text{SrFeO}_{3-\delta}$. Another significant contribution of this work is the observation of a high temperature magnetic anomaly, which was not seen earlier either in single crystals or polycrystals. This result assumes significance in the wake that no single author was able to fit the high temperature data (above T_N) to the Curie-Weiss law. Our serendipitous discovery of the presence of a high temperature feature through systematic ac susceptibility (χ_{ac}) and zero-field cooled, field-cooled magnetization ($M_{FC/ZFC}$) measurements, would explain this discrepancy. We believe that most authors may have overlooked its presence due to the standard perception of a paramagnetic behavior for $T > T_N$. Also, its presence might have been masked by the experimental data being measured at large temperature intervals.

II. EXPERIMENT

Samples of two different oxygen stoichiometries of SrFeO_3 were prepared by solid-state reactions. Starting materials of $\text{SrCO}_3, \text{Fe}_2\text{O}_3$ were weighed, thoroughly mixed in an agate mortar, and pre-fired at 1000 °C. The powders were again mixed and pressed into pellets of 12 mm diameter and were fired at two different temperatures. One pellet was fired at 1300 °C (Sample A) and the other was fired at a lower temperature of 1150 °C (Sample B). Both were sintered in flowing oxygen in a tube furnace, with a deliberately reduced oxygen partial pressure for Sample B, in order to impart greater oxygen loss and enhance the $\text{Fe}^{4+}/\text{Fe}^{3+}$ ratio. Oxygen stoichiometry was estimated by reducing SrFeO_3 to its basic oxide and elements, through the associated weight losses,

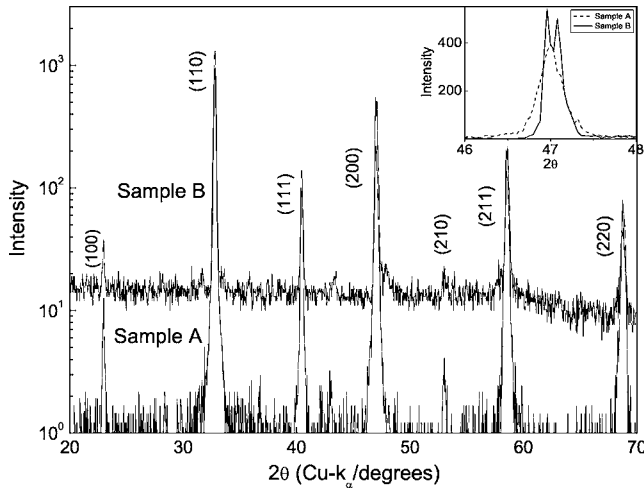


FIG. 1. X-ray diffraction pattern of Samples A and B Inset (a): enlarged spectrum of the (200) plane.

using thermogravimetry analysis (TGA) with an oxygen stoichiometric accuracy of around 0.03. X-ray diffraction (XRD) was used to characterize the structure and phase purity of the materials. Magnetization, magnetic susceptibility (dc and ac), resistivity and magnetoresistance measurements were carried out using a physical property measurement system (PPMS) from Quantum Design (San Diego, CA), as a function of temperature in the range, 10–300 K. Frequency was varied from 10 Hz–10 kHz in the ac susceptibility measurements at a fixed ac field amplitude of 10 Oe. Dc magnetization was done in fields ranging from 0 to 6 T with the samples cooled in zero field at different temperatures. Resistivity as a function of temperature was measured in zero field and at 6 T, using a standard four-probe technique.

III. RESULTS AND DISCUSSION

A. X-ray diffraction

X-ray diffraction patterns obtained for Samples A and B shown in Fig. 1 indicate a single SrFeO_3 phase without traces of impurities. A comparison of the spectra of Samples A and B with the ideal cubic perovskite of SrFeO_3 indicates a slight shift of Bragg reflections to lower angles indicating elongation of the unit cell. An expanded view of the (200) peak $2\theta_B \sim 47^\circ$ (inset Fig. 1), shows that Sample A has a shoulder indicating symmetry lower than that of the cubic SrFeO_3 . This signature of the pseudocubic phase continues through into Sample B which shows a clear splitting of the (200) reflection, indicating the advent of a tetragonal phase. Reports indicate the cubic \leftrightarrow tetragonal distortion to occur at $\delta=0.15$ and a strong split in the reflections of Sample B indicate an oxygen stoichiometry either close to or in excess of $\delta=0.15$.⁷ TGA showed a stoichiometry of $\delta=0.17$ for Sample A and a δ of 0.205 for Sample B.

B. AC magnetic susceptibility

Figure 2 shows variation of ac magnetic susceptibility (χ') as a function of temperature for samples A and B mea-

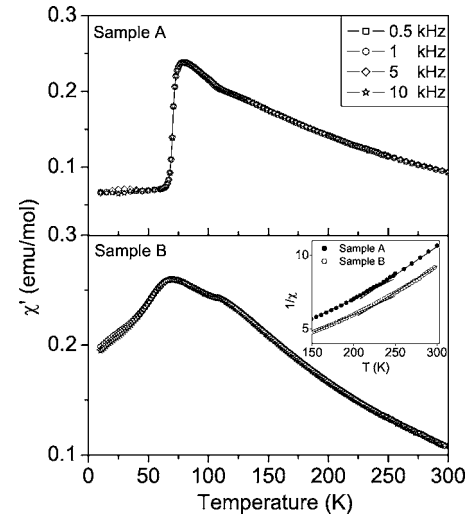


FIG. 2. Ac magnetic susceptibility as a function of temperature for (a) Samples A and (b) B. Inset shows $1/\chi$ versus T . The straight lines are guides to the eye showing the change in slope.

sured at different frequencies. With the lowering of temperature, Sample A (top panel) shows a transition around 78 K followed by a steep decrease in the magnetization down to 68 K. Further lowering of temperature results in a more gradual decrease in magnetization. Susceptibility curves at different frequencies show no variation and lie on top of each other through the entire temperature range of measurement. In addition to the transition around 78 K, another transition could also be seen as a cusp at around 120 K. These two transitions can be identified as the T (tetragonal, Fe^{3+} state) and a residual C (Cubic, Fe^{4+} state) phase, respectively. A closer look at χ_{ac} around 230 K reveals a weakly resolved cusp indicating a possible new magnetic anomaly.

Sample B however shows a clear cusp indicating the C phase around 110 K and a broad maximum (compared to Sample A) around 68 K indicating the T phase. The transition around 110 K in Sample B is strong when compared to a slope change seen in $\text{SrFeO}_{2.81}$. These features indicate the oxygen stoichiometry of Sample B is close to, but lower than, $\text{SrFeO}_{2.81}$. Resistivity measurements also confirm that Sample A has a composition just above that of $\delta=0.15$, and Sample B above that of $\delta=0.19$.

To confirm the weak anomaly seen in Fig. 2, $1/\chi_{ac}$ has been plotted as a function of temperature in the range 150–300 K (inset Fig. 2). A clear evidence of a slope change near this temperature is seen in both samples. These features show up as strong anomalies in the bulk magnetization measurements (χ_{dc}), which are discussed in the ensuing sections.

C. Resistivity and magnetoresistance

Figure 3 shows the resistivity and magnetoresistance curves measured at zero field and 6 T for Samples A and B. Resistivity increases as a function of temperature as Sample A [Fig. 1(a)] is cooled through its T phase transition temperature (~ 68 K) with a sudden increase at this temperature by at least an order of magnitude indicating the inter-relationship between the magnetization and transport anoma-

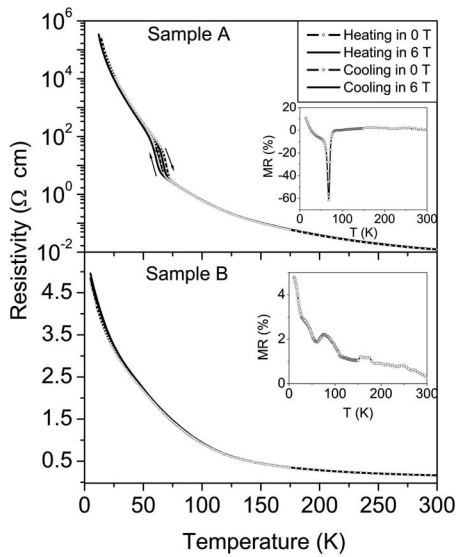


FIG. 3. Resistivity and magnetoresistance zero field and 6 T for (a) Samples A and (b) B as a function of temperature. Insets show the percentage change in resistance on the application of 6 T magnetic field.

lies. Resistivity increases exhibit a power-law behavior on further cooling. On heating, the sample shows a hysteresis around the ~ 68 K transition. No such anomaly is seen at the 120 K transition indicating that this antiferromagnetic ordering is not mediated by conduction electrons. An important observation is that we do not see any low temperature metallic phase. This is consistent with a decrease in Sample A's oxygen content and the $\text{Fe}^{4+}/\text{Fe}^{3+}$ ratio.

Application of a magnetic field of 6 T, suppresses the resistance of Sample A by more than 60% around the 68 K transition (inset of Fig. 3, top panel). The negative magnetoresistance continues well down to low temperatures, except for a small region between 10 and 20 K where it becomes positive. It is interesting to note that the shape of the magnetization curve is close to that of reported $\text{SrFeO}_{2.85}$ and the resistivity curve to that of $\text{SrFeO}_{2.81}$. These similarities along with values of δ obtained from TGA help us infer that the composition of Sample A falls between the reported $\text{SrFeO}_{2.85}$ and $\text{SrFeO}_{2.81}$.¹³

Resistivity of Sample B (Fig. 3, bottom panel) shows a monotonic insulating behavior from room to low temperatures. An interesting observation is that on the application of a 6 T magnetic field, the resistivity shows a positive magnetoresistance (see inset) of $\sim 5\%$ at 12 K. A fully insulating phase is only possible beyond the partly insulating $\text{SrFeO}_{2.81}$ phase and extending similar arguments to Sample B; it can be concluded that the composition of Sample B would fall above $\delta=0.19$. The tetragonal structural distortion of Sample B (Fig. 1 inset) also gives credence to this conclusion about the stoichiometry.

The effects of grain boundaries on the physical properties of the polycrystalline Samples A and B cannot be underestimated, in particular on the resistivity. A comparison of resistivity and magnetoresistance of the single crystal and polycrystalline CMR $\text{La}_{2/3}\text{Sr}_{1/3}\text{MnO}_3$ indicate that substantially

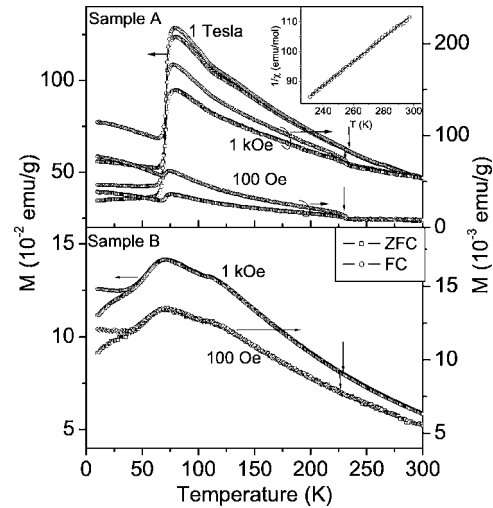


FIG. 4. Zero field cooled (ZFC) and field cooled (FC) measurements for Sample A at 1 T, 1 kOe, and 100 Oe, and for Sample B at 1 kOe and 100 Oe. A transition observed ~ 230 K is shown with arrows. For 1 T, a hysteresis around this temperature (marked with an arrow) can be seen.

higher values of resistivity and magnetoresistance were seen in polycrystalline samples fired at different temperatures. Magnetization on the other hand shows no difference, implying the considerable role played by the grain boundaries in the higher resistivity of the polycrystalline samples. Firing temperatures also decrease the resistivity, indicating a decreasing thickness of grain boundaries.¹⁴

The above finding also reveals that in a polycrystalline material, the potential barriers created by the oxygen nonstoichiometry can enhance the resistivity. As a comparison, Sample A has higher resistivity than that of single crystal $\text{SrFeO}_{2.81}$, whose oxygen stoichiometry is close to that of Sample A. However, the values of magnetoresistance (MR) in Sample A falls approximately between the compositions of single crystal $\text{SrFeO}_{2.85}$ and $\text{SrFeO}_{2.81}$ as reported by Lebon *et al.*¹³

The grain boundary effects did not appreciably affect the magnetic properties in either Sample A or B. This is confirmed from the comparison of Sample A with $\text{SrFeO}_{2.85}$ and $\text{SrFeO}_{2.81}$. The T_N of Sample A (78 K) falls between that of $\text{SrFeO}_{2.85}$ (~ 83 K) and $\text{SrFeO}_{2.81}$ (60 K).

D. Bulk magnetization

Figure 4 shows the zero-field cooled (ZFC) and field cooled (FC) dc magnetization measurements in the temperature range 10–300 K. For Sample A, ZFC data qualitatively shows all the features that are observed in the ac magnetic susceptibility (Fig. 1). The FC and ZFC curves are separate until about 230 K and merge above this temperature. The separation depends on the applied field and decreases as the field is increased to 1 T. The ZFC/FC curves of Sample B show a similar trend for different fields with the temperature at which the curves merge being 40 K for 100 Oe applied field.

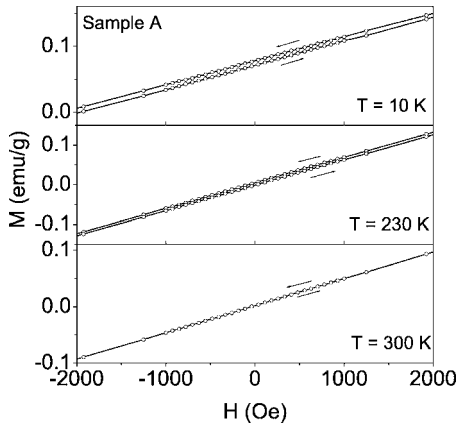


FIG. 5. Magnetization isotherms measured at different temperatures for Sample A. Only low field data is shown for clarity even though the data was acquired up to 6 T.

The ZFC curve measured at 100 Oe for Sample A shows a distinct kink around ~ 230 K, in addition to the anomalies observed at lower temperature. This is also seen in the ZFC as well as FC measurements at other fields (Fig. 4). This feature is completely unexpected, in view of the similar measurements carried out by many authors on this system.^{7,12,13} In order to explore this further, the magnetic hysteresis measured at different temperatures spanning a range from 10 to 300 K are shown in Fig. 5 for Sample A. At low temperatures (10 K) an extremely small loop could be seen, which does not saturate even at fields of 6 T. This is due to the presence of ferromagnetic interactions in the system. Note that there is a strong shift of the M - H curves away from the origin as the temperature is systematically lowered below 230 K. This tendency is associated with the coexistence of antiferromagnetic and ferromagnetic interactions and is typical in materials with helical magnetic ordering. For example, such loops are seen in MnSi which is a classic example of a helical magnet.¹⁵ Competing ferro- and antiferromagnetic effects due to the helical spin structure gives rise to a frustrated system similar to a spin glass and an unsaturated magnetization is caused by the spin fluctuations in the helical spin arrangement.

While the shift in the M - H loops due to exchange bias effects are expected below T_N which is 120 K for Sample A, the fact that we observe a systematic shift of the loops even up to 230 K indicates that the coexistence of competing magnetic order persists up to this temperature. This is an important observation that accounts for the difficulty experienced by researchers in fitting the high temperature data to standard models in this system. It is possible that due to the presence of this magnetic ordering at relatively high temperatures, attempts by several authors in past work to fit the susceptibility data above the Neél temperature to Curie-Weiss law resulted in poor fits that exhibit curvature. The inverse susceptibility (χ^{-1}) data above 230 K can be described by using the Curie-Weiss law $\chi = C/(T - \theta)$, and the fit to the data is shown in the Fig. 4 inset. The parameters obtained from the fit are $C = 2.47(1)$ and $\theta = 20.8(1)$ K. An effective moment μ_{eff} of $4.44\mu_B$, is obtained from the equation $\mu_{\text{eff}} = \sqrt{7.99C}$. This is somewhat smaller than $4.9\mu_B$ which is the spin-only value

for Fe^{4+} . In the case of Sample B, similar analysis yielded a larger effective moment ($4.9\mu_B$ as opposed to $4.44\mu_B$ for Sample A) indicating the increased contribution due to Fe^{3+} .

We can now put all these results in perspective and try to develop an understanding of magnetism and transport in these materials. It is known that the magnetic anomalies seen in this system are mainly due to the presence of varying proportions of $\text{Fe}^{4+}/\text{Fe}^{3+}$ content in oxygen deficient samples. Prior reports¹² also indicate the existence of fractional valence ($\text{Fe}^{3+\Delta}$) as a function of temperature that would profoundly affect the magnetic properties. This valence fluctuation adds to the complexity of a complete understanding of the strong correlation between electronic spin and charge leading to exotic magnetic and transport properties.

The sharp rise in resistivity of Sample A, thermal hysteresis, and associated magnetic anomalies are reminiscent of charge ordering (CO). In that sense, these systems have similarities to the perovskite oxide systems such as $\text{Pr}_{1-x}\text{Ca}_x\text{MnO}_3$ and $\text{La}_{1-x}\text{Sr}_{1+x}\text{MnO}_4$ which are known to exhibit charge ordering, large negative magnetoresistance, etc.^{16,17}

In Sample B, the oxygen deficiency is larger than that for Sample A which reduces the overlap of Fe-Fe orbitals even more. At the same time, the $\text{Fe}^{4+}/\text{Fe}^{3+}$ ratio changes because of an increase in Fe^{3+} which contributes to excess electrons in the e_g band. This combined effect results in insulating behavior albeit with a lower resistivity. No CO appears to occur in this sample with a logarithmic increase in resistivity with decreasing temperature.

The irreversibility in ZFC and FC curves in Sample A indicate the magnetic frustration induced by the competing effects of interlayer ferromagnetism (FM) and intralayer antiferromagnetic (AFM) order due to the helical magnetism. The degree of irreversibility is high for low applied fields and persists up to high temperatures as seen in Fig. 3(a). With increasing magnetic field, the degree of irreversibility decreases. This is consistent with the helical magnetic order that would transform to a collinear order at high fields. In SrFeO_3 a spin angle between neighboring $\{111\}$ planes has been found to be $\theta = 46^\circ$. Strong magnetic fields can decrease θ , reducing the irreversibility.¹⁸

In comparison, Sample B exhibits a smaller degree of irreversibility, which occurs only at low temperatures, indicating the reduced frustration and possible melting of the helical magnetic spin structure. This dilution of the helical spin structure is possible with increasing content of Fe^{3+} and its interaction with Fe^{4+} in $\text{SrFeO}_{3-\delta}$, which could yield an overall antiferromagnetic ordering.

We believe that the origin of the 230 K transition in Samples A and B result from the exchange interactions that dominate at temperatures between 70 and 230 K. The interactions are between Fe^{4+} -O- Fe^{4+} and Fe^{4+} -O- $\text{Fe}^{3+\delta}$, which are antiferromagnetic (former) and ferromagnetic (latter) in nature.¹⁹ The positive intercept of the Curie-Weiss fit, hysteresis in the M - H curves, and the shift of the overall M - H loops along the field axis observed in our data up to 230 K are all consequences of competing ferro- and antiferromagnetic effects. In the following section, we try to explain the occurrence of positive magnetoresistance in Sample B using

the model of the Mott insulator and variable range hopping of electrons in the localized energy levels.

E. Variable range hopping (VRH) conduction

The most notable aspect of the transport properties is the observation of a small positive magnetoresistance at low temperatures in Sample A and throughout the temperature range for Sample B. It is obvious that the increase in resistivity on the application of a magnetic field is related to the opening up of the gap between the bands or is due to the increased scattering of the electrons. The zero field resistivity and magnetization measurements point to a localized electron spin moment in Sample B, giving rise to a semiconducting behavior. Such antiferromagnetic insulators are classified as Mott insulators where a $M-I$ transition could occur due to electron correlations. Anderson pointed out that the disorder in a solid could introduce random potential energy in the lattice which ultimately leads to a localization of the electronic wave function.²⁰

At low temperatures Anderson localization occurs in many metals, semiconductors, and perovskite type oxides. The most striking examples of this category being high T_C superconductors and colossal magnetoresistance oxides like $\text{La}(\text{SrMn})\text{O}_3$.^{21,22} In those cases the conduction mechanism is governed by “variable range hopping” (VRH), where the hopping energy (W) varies with a temperature. The systems that undergo a VRH type of conduction follow the equation²³

$$\rho = \rho_0 \exp(T_0/T)^{1/(d+1)}. \quad (1)$$

In the above equation, “ d ” indicates the dimensionality of the hopping mechanism [$d=2$ and 3 imply a two-dimensional (2D) and 3D hopping conduction, respectively]. The above equation yields a straight line on a log scale with a slope of T_0 when fitted to the resistivity data. T_0 is a characteristic temperature related to the density of states $N(E_F)$ and the localization length (a) near the Fermi level given by²²

$$T_0 = 16/[a^3 k N(E_F)] \quad (2)$$

ρ_0 is a constant that depends on the electron-phonon interactions suggested by the relation

$$\rho_0 = (10/ve^2)[kT/a \cdot N(E_F)]^{1/2} \quad (3)$$

The hopping in VRH takes place between localized states in a small region close to E_F . Figure 6 shows the resistivity data fits to Eq. (1) in the temperature range 10–300 K for Sample B at zero and 6 T fields. A perfect fit to data was obtained with 3D VRH model. Interestingly, logarithmic resistivity data shows a linear rise at high temperatures (65–300 K,

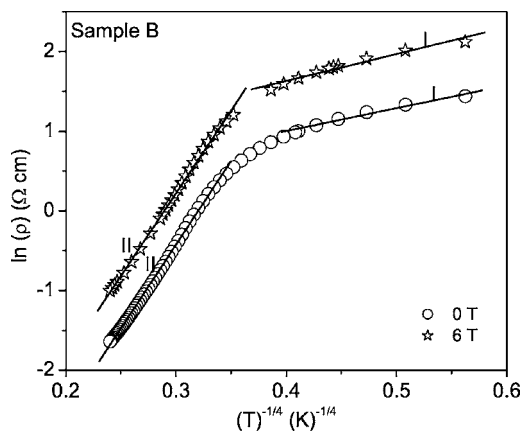


FIG. 6. Resistivity curves showing fit to variable range hopping model [Eq. (1)] in the temperature range 10–300 K for Sample B measured at 0 and 6 T. The crossover from regions I to II occurs around the magnetic anomaly shown in Fig. 2.

region II) followed by a transition to a smaller slope at low temperatures (10–30 K, region I) and each of these regions fit to the 3D VRH form of hopping conduction albeit with different slopes implying a varying localization length, a [Eq. (2)]. Intriguingly, this crossover from regions I to II occurs around the magnetic anomaly of Sample B (68 K). The double slope behavior is due to the multiphonon assisted hopping in different temperature regimes (regions I and II), which is seen in a few insulating High- T_C phases.²¹ In a solid with a high disorder a large network of varying potential barriers hamper the mobility of the electron and in such cases, the electron percolates through the network in a set of varied jumps than a single jump, assisted by the phonons to reach the final state. The energy necessary (W) is gained from the phonons and the electron attains its final state through the indirect hops assisted by the two levels of phonon energy. The necessary energy for a hop can be calculated using the relation²³

$$W = 3/[4\pi R^3 N(E_F)], \quad (4)$$

where R is the hopping distance in angstroms calculated from

$$R = (3a/[2\pi N(E_F)kT])^{1/4}. \quad (5)$$

The calculated values of T_0 , a , R , and W (R and W at 10 K) using Eqs (1) and (3)–(5) for Sample B in regions I and II at 0 and 6 T are given in Table I. Density of states at the Fermi level $N(E_F)$ was evaluated from the values given by Jaya *et al.*,²⁴ 28.365 states/Ry cell and a value of 3.6

TABLE I. Calculated values of T_0 , a , R , and W (at 10 K) for Sample B in regions I and II at 0 and 6 T.

Magnetic field (T)	Region I (10–30) K				Region II (75–300) K			
	T_0 (K)	a (Å)	R (Å)	W (meV)	T_0 (K)	a (Å)	R (Å)	W (meV)
0	67.370	0.425	0.284	28.8	1.95×10^5	2.98	0.146	2.11
6	130.20	0.341	0.270	34.0	1.84×10^5	3.04	0.147	2.08

$\times 10^{22}$ eV $^{-1}$ cm $^{-3}$. From the table it can be noted that increasing the magnetic field causes an increase in T_0 , which in turn causes a decrease in the localization length “ a .”

It is known that the spatial extension and the orbital overlap could decide the overall increase or decrease of resistance depending on which one is greater. A comparison between the localization lengths (a) of measured data at 0 and 6 T indicates that, the value of “ a ” at 6 T is smaller than that calculated for 0 T (Table I). A decrease in localization length directly affects the overlap integral resulting in the shrinkage of orbital overlap causing an increase of the resistance with field. On the other hand, at high temperatures the differences in the values of T_0 and a are marginal influencing the overall magnetoresistance, which is very small. Our above arguments provide concluding evidence to this effect, quantified by the model of Anderson localization in disorder solids.

Positive magnetoresistance seen in the perovskite $\text{La}_{2/3}\text{Ca}_{1/3}\text{MnO}_{3-\delta}$ was attributed to an increase in the gap by Barner *et al.*²⁵ Such a gap arises from the increase in the localized spin angle (θ) increasing the antiferromagnetic component as the $\theta \rightarrow \pi$. At $\theta=0$ the material is a ferromagnet. Magnetic interactions via polarized electrons which lead to double exchange are given by²⁶

$$E = -J_1 S \pm b \cos(\theta/2), \quad (6)$$

where θ is the angle between the localized spins, J_1 is the interatomic exchange energy, and b is the spin independent exchange integral.

When $\theta \rightarrow \pi$, in the $T-x$ phase diagram, x the carrier density progressively decreases, splitting the spin-up and spin-down bands, and opening up a gap, leading to an insulator behavior, as observed in Sample B.²⁴ With an increase

in magnetic field and with $N(E_F)$ remaining constant, in material showing positive magnetoresistance with a lower magnetization, the band gap further increases reducing the carrier density and enhancing the magnetoresistance. The low temperature positive magnetoresistance of Sample A may also occur due to a similar mechanism seen in Sample B.

IV. CONCLUSIONS

To conclude, we have investigated the electrical and magnetic properties of two insulating phases of $\text{SrFeO}_{3-\delta}$ due to oxygen deficiency, one with $\delta=0.17$ (Sample A) and the other with $\delta=0.205$ (Sample B). Negative magnetoresistance seen in Sample A is due to the conventional double exchange processes, whereas the low temperature positive magnetoresistance appears to arise from the opening up of the band gap due to the antiferromagnetic interactions. The most important finding of this investigation is the observation of a magnetic anomaly ~ 230 K, due to which the high temperature data at $T > T_N$ could not be fitted to a Curie-Weiss law. At low temperatures both of them behave as Mott insulators obeying variable range hopping type of conductivity. The varying valence state of Fe, plays a strong role in determining the electrical and magnetic properties in these ferrate systems.

ACKNOWLEDGMENTS

Work at USF is supported by DARPA through ARO Grant No. DAAD 19-03-1-0277. The authors wish to thank Dr. Serguei Koutcheiko, ICPET, Ottawa, Canada for the help in TG measurements. Financial support of this project by the National Research Council of Canada, in the NRC-Helmholtz collaborative program is gratefully acknowledged (NRCC-21-CRP-02).

*Corresponding author, Electronic mail: sharihar@cas.usf.edu

¹G. Briceno, H. Chang, X. Sun, P. G. Schultz, and X.-D. Xiang, *Science* **270**, 273 (1995).

²C. Zener, *Phys. Rev.* **82**, 403 (1951).

³A. J. Millis, P. B. Littlewood, and B. I. Shraiman, *Phys. Rev. Lett.* **74**, 5144 (1995).

⁴H. Roder, J. Zang, and A. R. Bishop, *Phys. Rev. Lett.* **76**, 1356 (1996).

⁵M. Uehra, S. Mori, C. H. Chen, and S.-W. Cheong, *Nature (London)* **399**, 560 (1999).

⁶T. Hotta and E. Dagotto, *Phys. Rev. B* **61**, R11879 (2000).

⁷P. K. Gallagher, D. N. Buchanan, and J. B. Mac Chesney, *J. Chem. Phys.* **41**, 2429 (1964); J. B. Mac Chesney, R. C. Sherwood, and J. F. Potter, *ibid.* **43**, 1907 (1965).

⁸A. E. Bocquet, A. Fujimori, T. Mizokawa, T. Saitoh, H. Namatame, S. Suga, N. Kimizuka, Y. Takeda, and M. Takano, *Phys. Rev. B* **45**, 1561 (1992).

⁹J. Mizusaki, M. Okayasu, S. Yamauchi, and K. Fueki, *J. Solid State Chem.* **99**, 166 (1992).

¹⁰J. J. Tunney, and M. L. Post, *J. Electroceram.* **5**, 63 (2000).

¹¹T. Takeda, Y. Yamaguchi, and H. Watanabe, *J. Phys. Soc. Jpn.* **33**, 967 (1972).

¹²Y. M. Zhao, R. Mahendiran, N. Nguyen, B. Raveau, and R. H. Yao, *Phys. Rev. B* **64**, 024414 (2001).

¹³A. Lebon, P. Adler, C. Bernhard, A. V. Boris, A. V. Pimenov, A. Maljuk, C. T. Lin, C. Ulrich, and B. Keimer, *Phys. Rev. Lett.* **92**, 037202 (2004).

¹⁴H. Y. Hwang, S.-W. Cheong, N. P. Ong, and B. Batlogg, *Phys. Rev. Lett.* **77**, 2041 (1996).

¹⁵K. Kadowaki, K. Okuda, and M. Date, *J. Phys. Soc. Jpn.* **51**, 2433 (1982)

¹⁶Y. Tomioka, A. Asamitsu, H. Kuwahara, Y. Moritomo, and Y. Tokura, *Phys. Rev. B* **53**, R1689 (1996).

¹⁷Y. Moritomo, Y. Tomioka, A. Asamitsu, Y. Tokura, and Y. Matsui, *Phys. Rev. B* **51**, 3297 (1995).

¹⁸S. Nakamura, and S. Iida, *Jpn. J. Appl. Phys., Part 2* **34**, L291 (1995).

¹⁹J. B. Goodenough, *Phys. Rev.* **100**, 564 (1955).

²⁰N. F. Mott, *Metal-Insulator Transitions* (Taylor & Francis, London, 1974), 2nd ed.

²¹R. K. Nkum, and W. R. Datars, *Phys. Rev. B* **46**, 5686 (1992); P. S. Prabhu, M. S. Ramachandra Rao, U. V. Varadaraju, and G. V. Subba Rao, *ibid.* **50**, 6929 (1994).

²²J. M. D. Coey, M. Viret, L. Ranno, and K. Ounadjela, *Phys. Rev.*

Lett. **75**, 3910 (1995).

²³N. F. Mott, and E. A. Davis, *Electronic Processes in Non-Crystalline Materials* (Clarendon, Oxford, 1979).

²⁴S. Mathi Jaya, R. Jagadish, R. S. Rao, and R. Asokamani, Phys.

Rev. B **43**, 13274 (1991).

²⁵K. Barner, P. Mandal, and R. V. Helholt, Phys. Status Solidi B **223**, 811 (2001).

²⁶P. W. Anderson, and H. Haswgawa, Phys. Rev. **100**, 675 (1955).